Journal of Power Sources 200 (2012) 14–20

Contents lists available at SciVerse ScienceDirect

Journal of Power Sources

journal homepage: www.elsevier.com/locate/jpowsour

# Solid oxide fuel cell with NiCo–YSZ cermet anode for oxidation of $CO/H_2$ fuel mixtures

Julie S. O'Brien, Javier B. Giorgi*

*Centre for Catalysis Research and Innovation, Department of Chemistry, University of Ottawa, 10 Marie Curie Prvt., Ottawa, Ontario, Canada K1N 6N5*

ARTICLE INFO

*Article history:*
Received 1 September 2011
Received in revised form 21 October 2011
Accepted 22 October 2011
Available online 25 October 2011

*Keywords:*
SOFC
Anode
Syngas
Hydrogen
Carbon monoxide
Cobalt
Nickel
Cermet

ABSTRACT

The suggestion has been made in the literature that solid oxide fuel cells (SOFCs) operated with syngas as fuel may be viable in certain gas ratio regimes. We have explored this hypothesis with a promising bimetallic anode material. SOFCs with $Ni_{0.7}Co_{0.3}$–YSZ cermet anodes were operated with $CO/H_2$ mixtures in the full concentration range. Electrochemical impedance spectroscopy and voltammetry measurements were employed to measure the exchange current density ($i_0$) values of each fuel mixture. The fuel mixtures of $CO/H_2$ ratios corresponding to the range 20/80 and 30/70 were found to have $i_0$ values larger than that of pure $H_2$ with the same cell. For these two fuel ratios, an improvement of 5–8 times, respectively, in the exchange current density has been observed. Higher $CO/H_2$ fuel ratios in the range of 60/40–80/20 produced $i_0$ values lower than $H_2$, as carbon poisoning is operational in this region. Continuous running of a cell with fuel ratio 25/75 $CO/H_2$ for 7 days produced $i_0$ values above the values for pure $H_2$ as has been recently suggested.



## 1. Introduction

Solid oxide fuel cells (SOFCs) are gaining a lot of interest due to their fuel flexibility, high fuel-electricity conversion efficiency, and long-term stability for practical applications [1,2]. Among many common fuels such as hydrogen, heavier liquid fuels such as alcohols (methanol, ethanol, etc.), hydrocarbons (methane, ethane, etc.) and biodiesel are being considered. At common operating temperatures for SOFCs (800–1000 °C), heavier liquid fuels undergo thermodynamic decomposition to form predominantly hydrogen and carbon monoxide [3,4]. Because of this, a greater understanding of how SOFCs utilize and tolerate different ratios of $H_2$ and CO is essential. Additionally, independently produced syngas can be used directly as a fuel.

With a mixture of $H_2$ and CO as fuel, each has a corresponding electrochemical oxidation reaction at the anode:

$$H_2 + O^{2-} \rightarrow H_2O + 2e^- \quad (1)$$

$$CO + O^{2-} \rightarrow CO_2 + 2e^- \quad (2)$$

In a recent computational paper, Andreassi et al. [5] found the contribution made by CO direct oxidation to be 12.5% for a cell running on a fuel ratio of 80/20 $CO/H_2$ at 800 °C with a Ni–8YSZ cermet anode. This effect becomes increasingly important at high current densities, where the model must consider both $H_2$ and CO direct oxidation in order to best simulate what is observed by experiment. Therefore, CO direct oxidation is present under SOFC operation conditions and is non-negligible.

With a mix of $H_2$ and CO in the fuel feed, the water–gas shift reaction (WGSR) must also be considered:

$$CO + H_2O \rightarrow CO_2 + H_2 \quad (3)$$

This equation shows that when appreciable concentrations of water vapour are present in the fuel feed, particularly at high fuel utilization, the CO concentration will be lowered and $H_2$ produced. The kinetics of this reaction are fast and favourable, much more so when compared to the direct oxidation of CO, so the presence of water vapour will cause the reaction to proceed, generating $H_2$. However, according to Andreassi et al. [5], considering only the WGSR (and not CO oxidation) underestimates the voltage given experimentally.

Traditionally, the most common anode material for SOFCs with a YSZ electrolyte layer is a Ni–YSZ cermet. Although Ni has a high activity for $H_2$ electrochemical oxidation, it is not an effective catalyst for CO oxidation. Additionally, because $H_2$ has a lower surface diffusion resistance on Ni when compared to CO, the amount of $H_2$ which can be oxidized is expected to be higher. This contributes to a rate constant which is 2–3 times higher at temperatures between

* Corresponding author. Tel.: +1 613 562 5800x6037; fax: +1 613 562 5170.
*E-mail address:* jgiorgi@uottawa.ca (J.B. Giorgi).

0378-7753/$ – see front matter © 2011 Elsevier B.V. All rights reserved.
doi:10.1016/j.jpowsour.2011.10.080

750 and 1000 °C for $H_2$ compared to CO on Ni–YSZ cermet anodes [6].

Carbon poisoning is a major concern when operating a cell with a Ni anode and a carbon-containing fuel due to the propensity for Ni to cause coke formation. With a CO fuel, two carbon deposition mechanisms must be considered:

$$2CO \rightarrow C + CO_2 \quad (4)$$

$$CO + H_2 \rightarrow C + H_2O \quad (5)$$

The first mechanism is the Boudouard disproportionation reaction [7,8] (Eq. (4)) in which CO is converted into carbon at the anode surface, thus both lowering the amount of CO available for electrochemical oxidation and causing carbon deposition on the anode surface. The second mechanism, Eq. (5), reduces CO using $H_2$ to produce carbon and water vapour. This carbon deposition also contributes to carbon poisoning of the anode, and the water vapour is likely to participate in the WGSR, thus consuming more CO fuel to produce $H_2$.

Some reported performances with Ni–YSZ based cermet anodes have shown a global trend: performance with a CO/$H_2$ mixed fuel, as measured by exchange current densities or power densities, produces intermediate values when compared to pure $H_2$ or CO fuel [5,6,9–11]. However, the trend between the higher pure $H_2$ value and the lower CO values is monotonic but not linear. The region with $H_2$ rich CO/$H_2$ fuel ratios can produce performance values much closer to the higher $H_2$ fuel, and CO rich CO/$H_2$ fuel ratios produce values closer to the lower CO fuel [6]. This observation (the "S" shaped curve) has been linked to the amount of carbon deposition which occurs at varying CO/$H_2$ fuel ratios. The largest cell deactivations reported in the literature [6,9,11,12] correspond to the 75/25 CO/$H_2$ fuel ratio range, where carbon deposition has been observed to occur in the largest quantities. Conversely, much lower carbon deposition occurs near 25/75 CO/$H_2$ fuel ratios. The lowest carbon deposition is observed for pure CO fuel [12]. This indicates that CO reduction by $H_2$ (Eq. (5)) is a possible mechanism for the carbon deposition.

Costa-Nunes et al. [10] observed a larger power density for a cell running on $H_2$ fuel at 700 °C with Cu–Co–$CeO_2$–YSZ anode when compared to its cobalt free analogue, Cu–$CeO_2$–YSZ. When the cell with Cu–Co–$CeO_2$–YSZ anode was run with 3 consecutive fuels, $H_2$, syngas, and CO, an increase in power densities was observed across this fuel series, in contrast with the nickel anodes. It was concluded that it was the addition of Co that produced an increasingly higher power density along this fuel gas series, in addition to the increased power density when running on pure $H_2$, relative to its Co free counterpart.

Since Ni–YSZ anodes are not effective in the direct oxidation of CO, and coking leads to poor performance with this fuel, in the present work we explore the addition of Co to a Ni catalyst to produce a NiCo–YSZ cermet anode which has recently shown promise in operation with other carbon containing fuels [13]. The synergistic effect of the two metals in the bimetallic NiCo alloy is expected to directly oxidize $H_2$ and CO respectively, producing a catalyst uniquely suited for this fuel mixture. The chosen Ni/Co ratio for this work was 70/30 due to success with this concentration of Co with previous systems containing sulfur [13–15]. Further tuning of the Ni/Co ratio in the anode cermet could result in even higher performances.

## 2. Experimental

Anode materials were synthesized containing a metal component comprising 55% by mass NiCoO of the total cermet material, with the mass balance of 8YSZ. The metallic component was synthesized to contain 70% Ni and 30% Co by mass, by a precipitation method described previously [16,17]. The fuel cell composition was determined by XRF and, following sintering, the metallic component of the cermet powder was confirmed as an alloy of NiCo as measured by powder XRD, as previously published [14]. Button cells were then manufactured for testing with cathode and reference electrodes of LSM, and pure Pt current collectors and leads. The total fuel flow used for all experiments was 50 sccm.

The fuel cell set-up has been described previously [13,15]. Briefly, the cell configuration used was a button cell with Pyrex® ring seals at the top of an alumina tube support. A potentiostat (VoltaLab®) was used to collect all electrochemical measurements at 800 °C, as measured by a K-Type thermocouple placed just above the counter electrode. In the construction of the setup, open circuit voltage (OCV) values greater than 1.1 V (for pure $H_2$ fuel) were considered as an indication of a properly working cell, sufficient to proceed with minimal current or molecular leakage.

The OCV was measured for 1 h during the reduction of the anode with hydrogen to produce the anode alloy metal: $Ni_{0.7}Co_{0.3}$–YSZ. The cell was then polarized with an anodic overpotential of 400 mV for 15 h during which time the metal reduction was completed and the anode was allowed to stabilize. A 2 h cycle of electrochemical impedance spectroscopy (EIS), voltammetry, and chronoamperometry (CA) was repeated 7 times to ensure the measurements used for literature reporting were stable and to observe any changes which occurred within the initial introduction of a new fuel. All values reported are taken from the final 2 h of measurement, which were found to be stable after the first ~6 h of measurement.

For EIS measurements, each spectrum was taken at OCV over the frequency range of 100 kHz to 250 mHz with an AC amplitude of 10 mV. The equivalent circuit used to fit impedance data was: $L_1R_1[R_2CPE_1[R_3CPE_2]]$. The equation used to obtain the exchange current density ($i_0$) values from the charge transfer resistance ($R_{CT}$, here set to be equal to $R_3$) values is the following, as derived from the low-field approximation of the Butler–Volmer equation: $i_0 = RT/nFR_{CT}$ [18]. Voltammetry measurements were obtained from 200 mV to 1100 mV of anodic overpotential at a scan rate of 2 mV $s^{-1}$. These values were set to ensure the region containing exchange current density information was collected. Exchange current density values from DC measurements were obtained from the Tafel plot and match qualitatively the values obtained from EIS measurements, as in previous work [14,15,19].

## 3. Results

### 3.1. OCV data at varying CO concentrations in $H_2$

Experiments were performed with varying CO/$H_2$ ratios following increasing and decreasing trends. The behavior is exemplified in Fig. 1 for two cells which show qualitatively the trends observed. For the cell designated as "cell 1", data for pure $H_2$ was collected

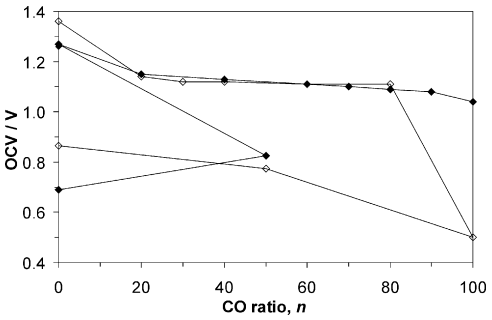


**Fig. 1.** OCV values for cell 1 (open symbols) and cell 2 (full symbols) collected at various CO/$H_2$ fuel ratios. The value of $n$, corresponds to the ratio of CO in the fuel inlet with a balance of $H_2$, where $n$ is given by the formula: $n_{CO}/(100 - n)_{H_2}$.

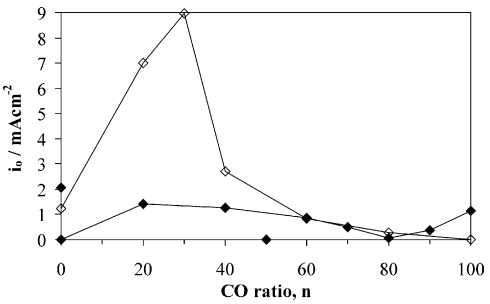


**Fig. 2.** Exchange current densities ($i_0$) values for cells 1 and 2 (open and closed shapes, respectively) collected at various $CO/H_2$ fuel ratios. The data is calculated from impedance spectra measurements (AC). For cell 2, the initial $H_2$ value is indicated at 2.1 mA cm$^{-2}$, followed by the next point with pure CO at 1.1 mA cm$^{-2}$. Decreasing amounts of CO in the fuel ratio then follow towards pure $H_2$. The value of $n$, corresponds to the ratio of CO in the fuel inlet with a balance of $H_2$, where $n$ is given by the formula: $n_{CO}/(100-n)_{H_2}$.

followed by increasing amounts of CO until pure CO was reached, at which point a measurement at 50/50 $CO/H_2$ was collected, followed by a return to pure $H_2$. For "cell 2", data for pure $H_2$ was initially collected for comparison purposes with "cell 1", then the fuel was switched rapidly to pure CO and the concentration of CO was systematically lowered until pure $H_2$ was collected. A further checkpoint at 50/50 $CO/H_2$ was then collected followed by a return to pure $H_2$.

The OCV values of the button cells are shown in Fig. 1. The initial OCV value for cell 1 (open symbols) with hydrogen is quite high at 1.36 V, as is expected with a low fuel utilization. The measurements made with varying mixtures of CO and $H_2$ appear to have a relatively constant value near 1.12 V. Exposure to pure CO gave a lower than expected value of 0.50 V, whereas returning to $H_2$ showed a small amount of recovery, but did not return to the original value for pure hydrogen, indicating possible carbon poisoning. The second button cell, cell 2 (full symbols) was also initially exposed to pure hydrogen and returned an OCV value of 1.26 V, similar to the first cell. In order to assess the reversibility of the data collection, the input fuel was immediately switched to pure CO followed by increasing amounts of $H_2$. Initially, with pure CO, an OCV value much closer to that according to the Nernst equation was obtained, 1.04 V. Excellent agreement was observed between cells 1 and 2 when exposed to varying $CO/H_2$ mixtures. The same plateau was observed with a similar constant value, indicating the independence of the order of data collection in relation to the chemical mechanism occurring. However, upon returning to a 50:50 mixture, a large drop in the OCV value was observed (~0.8 V) indicating an inability of both cells to tolerate fuel mixture cycling and the accumulation of carbon over time. This is also confirmed by the lowered final OCV point at 0.68 V in pure $H_2$.

### 3.2. Operation with varying CO concentrations in $H_2$

Impedance data was collected for the same two cells as previously described, in the same order of $H_2$ and CO ratios. Fig. 2 shows the exchange current densities obtained. The first cell initially showed an exchange current density value of 1.2 mA cm$^{-2}$ in pure hydrogen. For fuel feed ratios of 20/80 and 30/70 $CO/H_2$, the exchange current density values increased by a factor of 5.7 and 7.3 times respectively. This is a highly encouraging result, since these ratios of hydrogen and CO represent those of the thermal decomposition products expected at the operation temperatures of SOFCs for some common small molecules, such as $CH_3OH$, as well as possible fuel mixtures, such as $CH_3OH$ and $H_2$ [20,21]. These findings are also important since this is the first example of a Ni-based cermet anode producing exchange current densities which are larger for $CO/H_2$ fuel mixtures when compared to pure $H_2$. Cell 2 values for exchange current density in the 20/80 and 30/70 $CO/H_2$ region (after exposure to pure CO and increasing $H_2$ content) are comparable to those of the pure hydrogen collected initially. These values were not higher than that for initial pure hydrogen, likely due to cumulative carbon poisoning during measurements at higher CO concentration. The reasoning for this observation will be further discussed below.

The fuel ratio between 60/40 and 80/20 $CO/H_2$ is clearly a composition which results in poisoning, likely carbon poisoning. For cell 1, the exchange current density dropped below that of pure hydrogen for the first time. Continuing to a fuel composed of pure CO, and later 50/50 $CO/H_2$, and subsequently returning to pure hydrogen showed a complete loss of current output from all of these fuel compositions. It is proposed that poisoning by carbon in the 60/40 and 80/20 $CO/H_2$ fuel region is irreversible following the outlined fuel concentration program. Post-mortem examination of this cell showed a complete delamination of the porous anode cermet material from the non-porous YSZ electrolyte support disk, indicative of carbon poisoning.

The second cell showed an exchange current density in CO of 1.1 mA cm$^{-2}$, which is comparable to that of the initial hydrogen fuel. Following a decrease in the CO concentration in the fuel, the cell experienced a drop in exchange current density, producing values in excellent agreement with those of the first cell. This confirms that the low exchange current density values shown in the region of 60/40 and 80/20 $CO/H_2$ fuel are due to this fuel composition producing a carbon poisoning effect, not because of cumulative carbon deposition, as might be proposed for the first cell before collecting the "reverse" data for the second cell. Although a modest improvement was observed in the region of 20/80 and 30/70 $CO/H_2$, the exchange current density of this cell never exceeded that of the original pure hydrogen. The carbon poisoning in the higher CO concentration region is the likely reason for this observation. Similar to the first cell, returning to a composition of 50/50 $CO/H_2$ and pure hydrogen showed no current coming from the cell. Post-mortem examination of this cell was also impossible due to complete delamination of the porous anode cermet material.

As can be observed in the raw impedance spectra, Fig. 3, the initial data for both cells in hydrogen is highly comparable (all panels). However, the low CO concentration data for cell 1 (A) shows low charge transfer resistances compared to hydrogen. The serial resistance for the 20/80 and 30/70 $CO/H_2$ fuel is increasing compared to hydrogen. The reason for this initial increase is likely due to a small amount of surface carbon formation. For the low CO concentrations of cell 2 (B), the cell has already been exposed to the carbon poisoning region at high CO concentrations, so the series resistance is observed to be higher than that for the pure hydrogen, as previously observed for cell 1. However, the charge transfer resistance is also higher for this cell in the same fuel composition region. It is postulated that there is a larger amount of intercalated carbon in the lattice of the metallic phase, which would have the effect of increasing the charge transfer resistance (*vide infra*). For cells 1 and 2 at high CO concentration (C and D, respectively) an increase in both the charge transfer resistances and serial resistances can be observed when compared to hydrogen. This region is expected to have the highest capacity for carbon poisoning for reasons that will be discussed in Section 4. One important point to note is that cell 2, exposed to the high CO concentration and high carbon poisoning region (D) first experienced recovery when the CO concentration was lowered (B) to give impedance arcs much closer to that of the pure $H_2$ before the cell was exposed to any carbon sources.

It is important to note that the observations made from impedance data obtained at OCV are also applicable when impedance is collected at higher overpotentials. Inserts in Fig. 3 show EIS data at 200 mV. The Rs values are within error at both

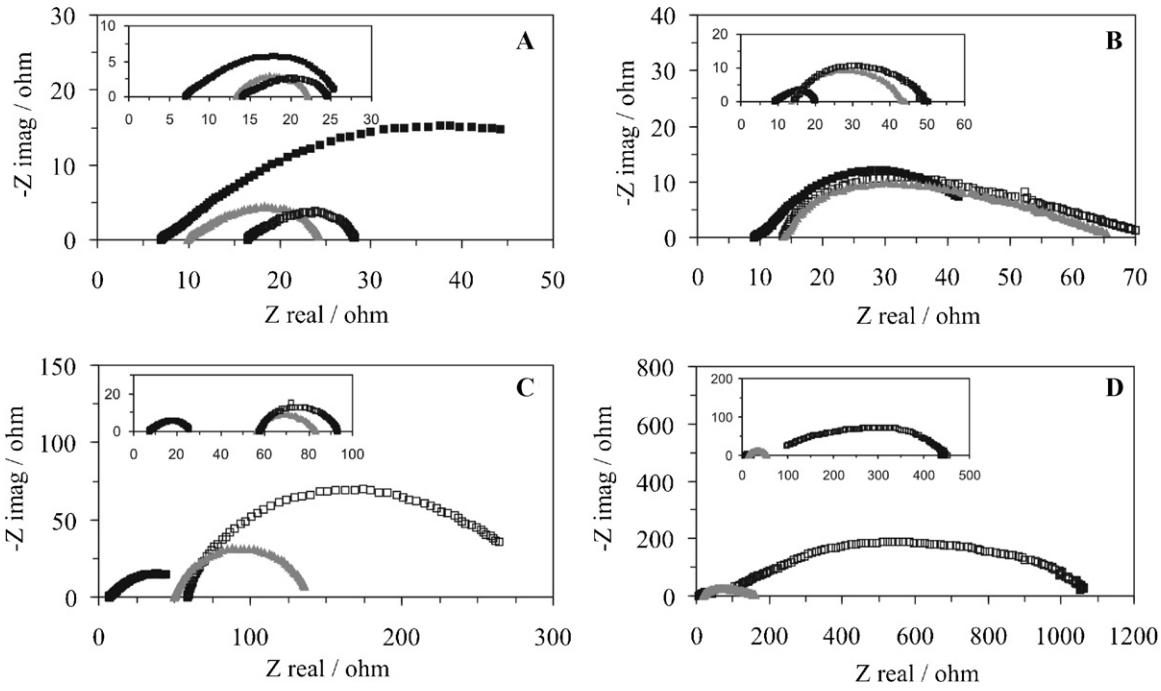


**Fig. 3.** Raw impedance data for cell 1 (Panels A and C) and cell 2 (Panels B and D). Data from pure $H_2$ (black squares), and low CO concentration, in the range 20/80 (open squares) to 30/70 (grey triangles) $CO/H_2$ is shown (Panels A and B). Data from pure $H_2$ (closed squares) and high CO concentration, in the range 60/40 (closed triangles) to 80/20 (open squares) $CO/H_2$ is shown (Panels C and D). Note the different vertical and horizontal axes between panels. Inserts show the EIS data at an overpotential of 200 mV.

potential settings and the $R_{CT}$ is lower at the higher overpotential, as expected.

Interspersed between electrochemical impedance spectral measurements, direct current cyclic voltammetry data was collected. The exchange current density values calculated from this data show identical trends as that of the EIS, however the values were more noisy than their EIS derived counterparts due the length of time needed to collect the cyclic voltammetry data as compared to the impedance data. Namely more microstructural changes can occur over the longer data collection period. The values obtained do, however, underscore the large increase in the exchange current density value with low $CO/H_2$ ratios, as seen with the EIS derived data.

Performance data was collected for each fuel mixture. The insert in Fig. 4 shows representative examples of polarization curves and power density data for three $CO/H_2$ fuel feeds. Although power values are necessarily small due to the three electrode configuration used in these experiments (requiring very thick electrolytes), the cells are well behaved. The main panel in Fig. 4 shows the maximum power density measured for each data set. Except for the first point in both series (pure hydrogen), the $P_{max}$ trend matches the trends observed in the measured exchange power densities as discussed above.

### 3.3. Long term performance with fuel ratio 25/75 $CO/H_2$

As discussed above, a fuel ratio of 25/75 provided enhanced performance. However, the presence of CO seemed to indicate a progressive carbon poisoning of the cell upon introduction of CO to the fuel mixture, particularly for high CO content. To test long term performance, a button cell was run for 7 days with the promising fuel mixture of 25/75 $CO/H_2$ following initial measurements with pure $H_2$. Fig. 5 shows the OCV and $i_0$ values observed.

A large OCV value, 1.25 V, was obtained for pure $H_2$, as expected (day 0), Fig. 5A. Following the addition of the 25/75 $CO/H_2$ fuel mixture, the OCV value dropped to a stable value of approximately 1.11 V (1.12 V for days 5–7). This small drop is not consistent with a simple reduction in the $H_2$ partial pressure, indicating that both $H_2$ and CO direct oxidation reactions are occurring simultaneously on the catalyst surface.

The corresponding exchange current density data is shown in Fig. 5B. The value shown here for $H_2$ (4.7 mA $cm^{-2}$) is slightly higher than that presented in Fig. 2 indicating a more robust button cell for this experiment. Nevertheless, the value is within the expected error range for the EIS derived $i_0$ comparing multiple cells. In agreement with trends observed for cells 1 and 2, *vide supra*, switching the fuel to a mixture of 25/75 $CO/H_2$ produced a rise in the $i_0$ value to 24.7 mA $cm^{-2}$ in day 1. This represents a 5.3 fold increase in $i_0$, again within error of other cells. However, despite this initial increase, the

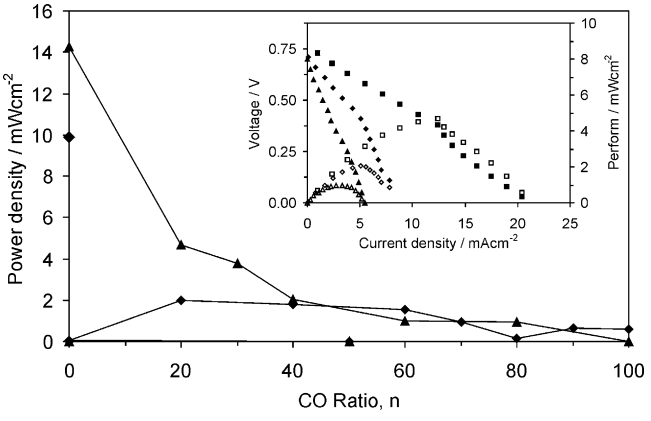


**Fig. 4.** Maximum power density values for cells 1 and 2 (triangles and diamond shapes, respectively) calculated at various $CO/H_2$ ratios. For cell 2, the initial $H_2$ value is indicated at 9.9 mW $cm^{-2}$ followed by the next point with pure CO at 0.59 mW $cm^{-2}$. Decreasing amounts of CO in the fuel ratio then follow towards pure $H_2$. The value of $n$, corresponds to the ratio of CO in the fuel inlet with a balance of $H_2$, where $n$ is given by the formula: $n_{CO}/(100 - n)_{H_2}$. *Insert*: Sample of performance data for cell 1 with $CO/H_2$ fuel ratios of 20/80 (squares), 40/60 (diamonds), and 60/40 (triangles). Voltage data is shown as closed shapes, whereas power density data is shown as open shapes.

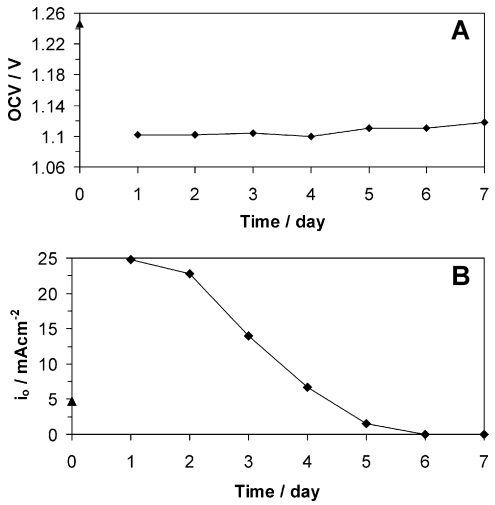


**Fig. 5.** Fuel cell run continuously for 9 days. Following $H_2$ measurements for 2 days (day 0, triangle), a fuel ratio of 25/75 $CO/H_2$ was run for 7 days (days 1–7, diamonds). (A) OCV values (B) $i_0$ values derived from electrochemical impedance data.

$i_0$ values observed fell below the value found for pure hydrogen at days 5 and 6, and finally approached zero after 7 days of testing at the 25/75 $CO/H_2$ fuel ratio. Despite this eventual fall in performance, the initial 25/75 $CO/H_2$ fuel ratio data showed a significant increase in performance when compared to pure $H_2$; therefore, further research to prolong this higher performance area would yield important SOFC progress.

### 3.4. Scanning electron microscopy of post-run anode material

Post-run micrographs of the anode following 7 days running with a fuel mixture of 25/75 $CO/H_2$ are shown in Fig. 6. Due to complete delamination of the current collector from the YSZ electrolyte disk following the 7 day run, a post-run cross sectional image was impossible to collect. However, it was possible to collect anode material which remained attached to the current collector, mount the powder sample onto carbon tape, and image it by SEM.

In Fig. 6, Panel A shows the agglomerate configuration with a size range from tens to hundreds of microns. Panel B outlines the particle sizes which range from approximately 0.1–2 microns. A small amount of charging is seen (bright particles) likely due to the low electron conductivity of YSZ-rich particles furthest from the carbon tape mount. Pores ranging in sizes similar to the particle size stated above can be seen with no visible carbon obstructions. Both at low magnification, Panel A, and higher magnification, Panel B, there is no evidence for visible, organized carbon structures such as microtubes or microrods, which might have grown under the outlined fuel cell conditions during this extended run. Such structures are typical and have been observed with Ni and Co anodes under methane and other carbon containing fuels [15,22–25]. General carbon buildup was not observed either by imaging or by EDS where the carbon signal could not be distinguished from the typical adventitious carbon. Therefore, no direct SEM evidence to support the uncontrolled formation of coke on the anode could be found; however, due to the loss of exchange current density with time, and the complete delamination of the anode and current collector from the YSZ electrolyte disk, it can be hypothesized that preferential reactivity of different sites may lead to anode delamination. Due to the apparent physical breakdown of the anode in this region, no material was able to be recovered for direct imaging.

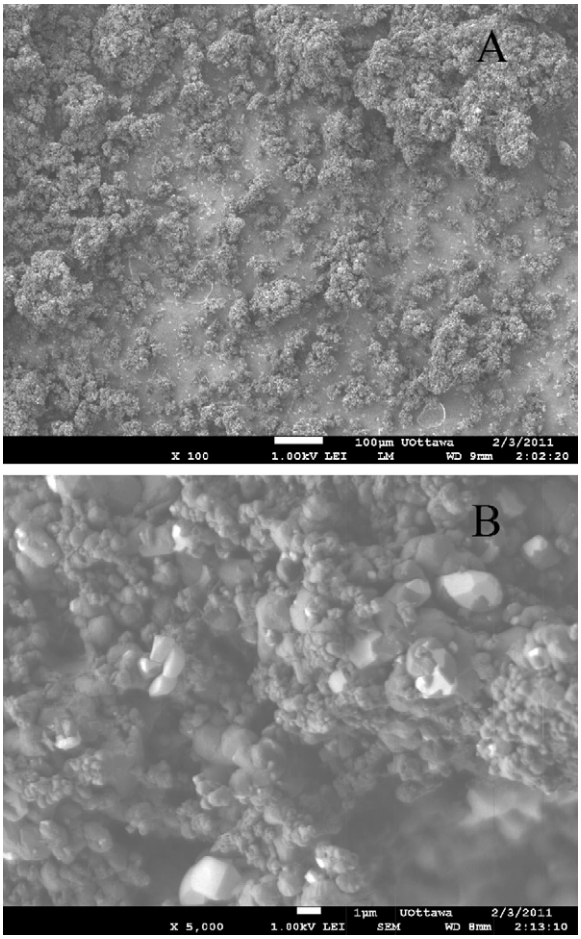


**Fig. 6.** Scanning electron micrograph of the $Ni_{0.7}Co_{0.3}$–YSZ anode material post-run following the 7 day run with a fuel mixture of 25/75 $CO/H_2$. Panel A shows a magnification of 100× with a measurement bar of 100 μm, and Panel B shows 5000× with a measurement bar of 1 μm. The powder sample was mounted on carbon tape.

## 4. Discussion

Drawing from the OCV data, the value for pure $H_2$ is slightly higher than expected. This is likely due to the trend in increasing OCV with decreasing fuel consumption, and the expected low fuel consumption with the high fuel flow rate utilized. Also at low fuel consumption, the concentration of products is expected to be extremely low, lending to a very small term in the Nernst equation. The plateau at a slightly lower value than pure $H_2$ for all $CO/H_2$ fuel mixtures is indicative of a constant ratio of reactions occurring over this entire range. With a rate approximately 3 times slower than that of $H_2$, the oxidation of CO is expected, especially at higher potentials, to produce $CO_2$. As shown by Andreassi et al. [5] the oxidation of CO is a factor which cannot be neglected when considering the global mechanism with a $CO/H_2$ fuel mixture. Carbon monoxide adsorbed on nickel does not have favourable desorption thermodynamics [26]. It is likely either to undergo an electrochemical oxidation to form surface $CO_2$ followed by desorption to the gas phase, or disproportionation via the Boudouard reaction to contribute to carbon poisoning (Eq. (4)). Carbon formation on the surface can also occur via CO reduction (Eq. (5)). The direct oxidation of CO is expected to give an OCV of 0.98 V [5]. The value obtained of 1.04 V is within expected error and follows the rule of highest expected OCV with low fuel consumption. The values for the 50/50 $CO/H_2$ data point show reasonable agreement.

Impedance spectra indicated important trends for the exchange current density at each fuel composition. The most noteworthy

observation is that the data produced larger exchange current densities in the 20/80 and 30/70 $CO/H_2$ fuel composition range. This cell had not yet experienced the carbon poisoning range between 60/40 and 80/20 $CO/H_2$ fuel. Although the direct electrochemical oxidation of $H_2$ on Ni is approximately 2–3 times faster than on Co [6], it is proposed that Co sites in the alloy are responsible for CO oxidation. This observation has been recorded previously for a Cu–Co–$CeO_2$–YSZ anode when compared to the Co-free Cu–$CeO_2$–YSZ equivalent cell [10]. In this work, the cell containing Co also gave activities 5–8 times higher for CO when compared to $H_2$.

For the carbon poisoning range between 60/40 and 80/20 $CO/H_2$, two carbon poisoning mechanisms can be proposed. It is difficult to assess to what extent these two mechanisms occur in the present system, since post-mortem examination of the button cell by SEM was not possible due to anode delamination. The first mechanism states that carbon deposited on the surface can block active catalyst sites. Since catalysis occurs preferentially on more energetic edge, step and kink sites, it is reasonable to assume that these could be poisoned more quickly, resulting in a large decrease in overall catalyst activity [27]. The second carbon poisoning mechanism is the intercalation of carbon into the bulk of the metal. This can have a large effect in decreasing the overall conductivity of the metallic phase of the anode cermet, which would greatly lessen the amount of current output observed. In addition to this, intercalation of carbon causes an expansion of the metal lattice, resulting in an increase in particle size. This can cause a sintering-like effect to reduce anode surface area and pore volume, thus reducing anode activity. Carbon intercalation is the first step in metal dusting [28,29], which is known to occur more aggressively at the grain boundaries resulting in the degradation of the anode microstructure.

The amount of surface carbon poisoning can be reduced by the addition of water into the fuel stream, but this has only shown a small ability to remove a significant amount of carbon [30]. The reaction with the fastest expected rate is the electrochemical oxidation of $H_2$ on Ni surface. Since this reaction produces a small amount of water, it is expected to result in a small amount of the water gas shift reaction to occur, which has very fast kinetics on the Ni surface producing additional usable hydrogen. However, it is known that the presence of water vapour can lead to a decrease in OCV. Since the OCV was observed to be very high, this reaction is expected to occur in negligible amounts. The presence of both CO and $H_2$ in the fuel stream allow for CO reduction to occur producing carbon, Eq. (5). At the high operation temperatures used, a small amount of CO disproportionation via the Boudouard reaction, Eq. (4), to produce elemental carbon is also expected.

As described previously [14], the effect of the addition of Co to the Ni cermet anode in the ratio of 70/30 Ni/Co has clear synergistic effects. The alloy produced a higher exchange current density with hydrogen fuel than either metal alone, and higher than the sum of both metal contributions. Furthermore, when operated with pure methane fuel, the nickel anode cells experienced failure within a few hours while the alloy anode cells were able to operate for longer periods (although poisoning ultimately occurred). However, with the addition of a fuel mixture of 10% v/v $H_2S/CH_4$, this alloy anode composition experienced an improvement in exchange current density which exceeds that of a Ni cermet anode both in the ratio of improvement of performance (namely $[i_0H_2S/CH_4]/i_0H_2$) and in the absolute performance value for the sulfidated hydrocarbon fuel. This provides strong evidence of the positive synergistic effect of Co in the outlined composition with Ni, as can be observed herein.

The long term effects of running a button cell at the $CO/H_2$ concentration, which produced the highest $i_0$ values (25/75) was investigated. Days 1–3 produced $i_0$ values significantly higher than pure $H_2$ fuel. It is proposed that a synergistic effect of the NiCo alloy in the anode produces optimal conditions for the oxidation of both fuels in this particular ratio. It is possible that the similarity in the two ratios, 25/75 $CO/H_2$ fuel, and 30/70 Co/Ni alloy is a key to this observed initial increase in $i_0$ values. That is, that CO is preferentially oxidized on Co sites of the alloy and hydrogen is oxidized on Ni sites and the concentration relates to the relative rates of oxidation and surface mobility of the two gases. Nevertheless, by day 4, the observed $i_0$ values were comparable to that of pure $H_2$, and finally by day 7, it had fallen to approximately zero.

No visible, organized carbon structures were observed following the post-run microscopy of the anode exposed for 7 days under 25/75 $CO/H_2$ fuel conditions. Since this fuel ratio has been previously reported to produce low coking, our observations further confirm this statement. However, if surface carbon poisoning with the formation of organized, visible structures is not prevalent in this regime, a different mechanism must cause the eventual degradation of the fuel cell. It is hypothesized that preferential reactivity of different sites may give rise to a change in the anode microstructure over time under operating conditions. The more active step sites are known to give rise to CO dissociation [31], which with the presence of hydrogen to remove the molecular oxygen, represents a source for carbon [32]. A microprocess such as metal dusting [28,29] is a possible explanation for the lack of visible carbon in the post-mortem SEM images. Metal dusting is known to occur more aggressively at the grain boundaries, which coupled with a high $CO/H_2$ ratio, can result in the degradation of the anode microstructure by loss of grain boundary contacts important in the physical integrity of the anode. This change eventually prevents the proper electrical contact between the anode cermet and the current collector mesh.

## 5. Conclusions

A cermet anode of alloyed NiCo–YSZ has been discovered to give higher exchange current density values for low ratio of $CO/H_2$ fuels in the range 20/80 and 30/70 compared to pure $H_2$. This is the first example of a Ni-based anode providing higher performance with a $CO/H_2$ mixed fuel than for a pure $H_2$ fuel. It is postulated that the reason for this is the synergetic behavior between the Co and Ni in the CoNi alloy of the cermet via preferential reactivity. This system would have industrial applications since it combines both two available fuels, $H_2$ and CO, and two relatively inexpensive metals, Ni and Co. Lower performances when compared to pure $H_2$ fuel were observed for high ratios of $CO/H_2$ in the range 60/40–80/20. It is expected that carbon poisoning in this range contributed to the lowered values. Finally, continuous running of a cell with fuel ratio 25/75 $CO/H_2$ for 7 days produced $i_0$ values, which were observed to increase significantly above the values for pure $H_2$ during days 1–4, but fell below this value during subsequent days. No visible coking was observed leading to the hypothesis that changes in mictrostructure of the anode cermet are the cause for the loss of exchange current density.

## Acknowledgements

The authors are grateful for financial support provided by the Natural Sciences and Engineering Research Council of Canada (NSERC), the Ontario Research Fund (ORF-RE), and the Ontario Fuel Cell Research and Innovation Network (OFCRIN).

## References

[1] S. McIntosh, R.J. Gorte, Chem. Rev. 104 (2004) 4845–4865.
[2] A.B. Stambouli, E. Traversa, Renew. Sustain. Energy Rev. 6 (2002) 433–455.
[3] J.H. Koh, B.S. Kang, H.C. Lim, Y.S. Yoo, Electrochem. Solid-State Lett. 4 (2001) A12–A15.

[4] M.F. Liu, R.R. Peng, D.H. Dong, J.F. Gao, X.Q. Liu, G.Y. Meng, J. Power Sources 185 (2008) 188–192.
[5] L. Andreassi, C. Toro, S. Ubertini, J. Fuel Cell Sci. Technol. 6 (2009), 021307-021301–021307-021315.
[6] Y. Matsuzaki, I. Yasuda, J. Electrochem. Soc. 147 (2000) 1630–1635.
[7] O. Boudouard, C.R. Hebd, Seances Acad. Sci. 148 (1909) 348–351.
[8] Y. Tang, J. Liu, Int. J. Hydrogen Energy 35 (2010) 11188–11193.
[9] K. Sasaki, Y. Hori, R. Kikuchi, K. Eguchi, A. Ueno, H. Takeuchi, M. Aizawa, K. Tsujimoto, H. Tajiri, H. Nishikawa, Y. Uchida, J. Electrochem. Soc. 149 (2002) A227–A233.
[10] O. Costa-Nunes, R.J. Gorte, J.M. Vohs, J. Power Sources 141 (2005) 241–249.
[11] X.F. Ye, S.R. Wang, J. Zhou, F.R. Zeng, H.W. Nie, T.L. Wen, J. Power Sources 195 (2010) 7264–7267.
[12] V. Alzate-Restrepo, J.M. Hill, J. Power Sources 195 (2010) 1344–1351.
[13] J.S. O'Brien, J.B. Giorgi, ECS Trans. 28 (2010) 221–231.
[14] C.M. Grgicak, M.M. Pakulska, J.S. O'Brien, J.B. Giorgi, J. Power Sources 183 (2008) 26–33.
[15] C.M. Grgicak, R.G. Green, J.B. Giorgi, J. Power Sources 179 (2008) 317–328.
[16] C.M. Grgicak, R.G. Green, W.F. Du, J.B. Giorgi, J. Am. Ceram. Soc. 88 (2005) 3081–3087.
[17] C.M. Grgicak, R.G. Green, J.B. Giorgi, J. Mater. Chem. 16 (2006) 885–897.
[18] B. Kenney, K. Karan, J. Electrochem. Soc. 153 (2006) A1172–A1180.
[19] C.M. Grgicak, J.B. Giorgi, J. Phys. Chem. C 111 (2007) 15446–15455.
[20] M. Cimenti, J.M. Hill, J. Power Sources 186 (2009) 377–384.
[21] K. Sasaki, K. Watanabe, K. Shiosaki, K. Susuki, Y. Teraoka, Elec. Soc. Proceedings 2003, 2003, pp. 1295–1304.
[22] R.T.K. Baker, M.A. Barber, P.S. Harris, F.S. Feates, R.J. Waite, J. Catal. (1972) 51–62.
[23] R.T.K. Baker, P.S. Harris, J. Henderson, R.B. Thomas, Carbon 13 (1975) 17–22.
[24] R.T.K. Baker, P.S. Harris, S. Terry, Nature 253 (1975) 37–39.
[25] C.W. Keep, R.T.K. Baker, J.A. France, J. Catal. 47 (1977) 232–238.
[26] M. Shishkin, T. Ziegler, J. Phys. Chem. C 113 (2009) 21667–21678.
[27] C.M. Chun, J.D. Mumford, T.A. Ramanarayanan, J. Electrochem. Soc. 147 (2000) 3680–3686.
[28] E. Pippel, J. Woltersdorf, R. Schneider, Mater. Corros. 49 (1998) 309.
[29] H.J. Grabke, Mater. Corros. 49 (1998) 303.
[30] A. Weber, B. Sauer, A.C. Muller, D. Herbstritt, E. Ivers-Tiffee, Solid State Ionics 152 (2002) 543–550.
[31] E. Bjorgum, D. Chen, M.G. Bakken, K.O. Christensen, A. Holmen, J. Phys. Chem. B 109 (2005) 2360.
[32] J. Engbaek, O. Lytken, J.H. Nielsen, I. Chorkendorff, Surf. Sci. 602 (2008) 733.